1448 *Biochemistry* **2010,** *49,* 1448–1459
DOI: 10.1021/bi901855z

BIOCHEMISTRY
including biophysical chemistry & molecular biology
Article

Inverse Correlation of Thermal Lability and Conversion Efficiency for Five Prion Protein Polymorphic Variants[†]

Louise Kirby,[‡] Sonya Agarwal,[‡] James F. Graham,[‡] Wilfred Goldmann,[§] and Andrew C. Gill*[,‡]

[‡]*Neuropathogenesis Division, The Roslin Institute and Royal (Dick) School of Veterinary Studies, The Alexander Robertson Building, Easter Bush Veterinary Centre, Roslin, Midlothian EH25 9RG, U.K., and* [§]*Neuropathogenesis Division, The Roslin Institute and Royal (Dick) School of Veterinary Studies, University of Edinburgh, Roslin, Midlothian EH25 9PS, U.K.*

Received October 29, 2009; Revised Manuscript Received January 19, 2010

ABSTRACT: Transmissible spongiform encephalopathies (TSEs) are associated with the accumulation of deposits of an abnormal form, PrP^{Sc}, of the host-encoded prion protein, PrP^{C}. Amino acid substitutions in PrP^{C} have long been known to affect TSE disease outcome. In extreme cases in humans, various mutations appear to cause disease. In animals, polymorphisms are associated with variations in disease susceptibility and, in sheep, several polymorphisms have been identified that are known to affect susceptibility of carriers to disease. The mechanisms of polymorphism-mediated modulation of disease susceptibility remain elusive, and we have been studying the effect of various amino acid substitutions at PrP codon 164 (mouse numbering), in the $\beta2-\alpha2$ loop region of the prion protein, to attempt to decipher how polymorphisms may affect disease susceptibility. Combined *in vitro* approaches suggest that there exists a correlation between the ability of protein variants to convert to abnormal isoforms in seeded conversion assays versus the thermal stability of the protein variants, as judged by both thermal denaturation and an unseeded *in vitro* oligomerization assay. We have performed molecular dynamics simulations to give an indication of backbone conformational changes as a result of amino acid changes and found that alteration of a single residue in PrP can result in local changes in structure that may affect global conformation and stability. Our results are consistent with modulation of disease susceptibility through differential protein stability leading to enhanced generic misfolding of TSE resistance-associated protein variants.

The transmissible spongiform encephalopathies (TSEs)[1] constitute a family of fatal, neurodegenerative disorders that include scrapie in sheep, bovine spongiform encephalopathy (BSE) in cattle, and Creutzfeldt−Jakob disease (CJD) in humans. Characteristics of disease include neuronal cell death, spongiform degeneration, and astrocytic gliosis leading to a variety of clinical manifestations including weight loss, puritus (in sheep), dementia (in humans), and ataxia leading ultimately to death. The principal molecular event in TSE disease appears to involve a conformational transition in a ubiquitous host protein, the prion protein or PrP^{C}, that leads to accumulation of an abnormal form, PrP^{Sc}, in insoluble aggregates (*1*). The two prion protein isoforms appear to have identical covalent structures, but PrP^{Sc} has significantly increased levels of β-sheet compared to PrP^{C} (*2*). The abnormal form is partially resistant to proteases resulting in it increasing in abundance in the brains of TSE-affected individuals where it forms insoluble plaques and fibrils. Furthermore, the prion hypothesis suggests that this form is sufficient to transmit disease to naive individuals, where it propagates its structure on nascent PrP^{C} molecules (*3*).

The prion protein has been shown to be the product of the *prnp* gene (*4*). In common with other protein misfolding disorders in humans, various mutations within the *prnp* gene have been identified that appear to result in spontaneous TSE disease. Familial TSE diseases are inherited in an autosomal dominant manner and imply a direct correlation between the prion protein and disease; however, the mechanisms that underlie these familial diseases have yet to be established. In addition to apparently disease-causing mutations, polymorphisms have been identified in human, ovine, caprine, murine, and cervine *prnp* genes, among others, that appear to exert substantial effects on susceptibility of individuals to infection with exogenous TSE agents. For example, to date, all clinical cases of variant CJD (vCJD) infection have involved humans homozygous for methionine at codon 129 of the PrP protein, while those homozygous for valine appear significantly more resistant, and heterozygotes may be as susceptible as methionine homozygotes (*5*, *6*). For many years, polymorphisms in the ovine *prnp* gene at codons 136, 154, and 171 have been known to control susceptibility to both natural and experimental TSE infection. Sheep that are homozygous for the VRQ allele of PrP (where each letter represents that single-letter amino acid code at positions 136, 154, and 171) succumb to natural scrapie with almost 100% incidence in infected flocks, while ARR homozygous sheep appear to be almost entirely resistant (*7*). Interestingly, a recently identified "atypical" form of scrapie targets sheep with a pattern of susceptibility that is essentially the reverse of this; those sheep traditionally associated with resistance to

[†]This work was partially funded by project grants from BBSRC, USDA, and DEFRA. J.F.G. was supported by a doctoral training grant from BBSRC.

*To whom correspondence should be addressed. Tel: +44 (0) 131 651 7310. Fax: +44 (0) 131 440 0434. E-mail: Andrew.gill@roslin.ed.ac.uk.

[1]Abbreviations: BSE, bovine spongiform encephalopathy; CD, circular dichroism; CFCA, cell-free conversion assay; CJD, Creutzfeldt−Jakob disease; MD, molecular dynamics; PK, proteinase K; PrP-res, proteinase K resistant prion protein; PrP^{C}, cellular prion protein; PrP^{Sc}, scrapie-associated prion protein; Rec-PrP, recombinant PrP; rms, root mean squared; SAF, scrapie-associated fibrils; SEC, size exclusion chromatography; TSE, transmissible spongiform encephalopathy.

 Published on Web 01/19/2010

classical scrapie are most susceptible to atypical scrapie and vice versa. Thus, polymorphism-mediated susceptibility to disease is TSE strain-dependent, a property identified in mice many years previously (*8*). As with disease-causing mutations, the mechanisms that underlie these effects are yet to be established but may represent differential stabilization of the structures of PrP^{C}, PrP^{Sc}, or some intermediate form. Polymorphisms may also affect any interaction between PrP^{C} and PrP^{Sc} or may be involved in interactions with accessory molecules, such as the putative chaperone protein X (*9*).

We have recently discovered a novel polymorphism within the sheep *prnp* gene at codon 168 (*10*). A small number of sheep were identified in which the wild-type amino acid, proline, was replaced with leucine in one of the two *prnp* alleles, resulting in animals heterozygous for the amino acid substitution. We noted that this amino acid change appears to prolong the incubation period against experimental BSE infection (*10*), and the amino acid change also modulates conversion of the prion protein to a proteinase K (PK) resistant isoform (PrP-res) in a cell-free conversion assay (CFCA) (*11*). In addition, the equivalent substitution in murine recombinant PrP (codon 164 is the equivalent codon using murine numbering, which will be used from this point forward unless otherwise stated) produces a protein that is also resistant to conversion in our cell-free conversion assay, using a murine-passaged scrapie strain, 87V, as seed. Thus, we have determined that this particular amino acid has an important role in directing conversion efficiency of PrP in two different species and against two different TSE strains (*11*).

The current work aims to investigate further the mechanistic aspects of susceptibility/resistance mediated by codon 164, as a model for other polymorphic sites in PrP. To do this, we have generated recombinant PrP in which the proline, normally expressed at codon 164, was replaced with four different amino acids (Leu, Glu, Gln, and Ser). We studied the folding and misfolding characteristics of the resulting proteins and have also undertaken molecular dynamics (MD) simulations of the equivalent protein variants to assess whether the amino acid changes alter the structure of the normal, α-helical form. Crucially, for five related proteins we found a positive correlation between susceptibility to *in vitro* conversion and protein stability. Conversely, using two proteins we find to be at extremes of the stability spectrum, we show that the protein that is thermally least stable oligomerizes faster than the wild-type protein, which we found to be thermally most stable. By use of molecular dynamics simulations, we also predict that conformations in the vicinity of the polymorphism vary subtly depending on the incorporated amino acid, suggesting that stability may be mediated by variations in protein backbone structure and changes in the side chain hydrogen bonding that result. Our data support the hypothesis that resistance-associated prion proteins misfold more readily and, hence, may have a shorter half-life in uninfected animals, thereby reducing apparent substrate during TSE disease.

MATERIALS AND METHODS

Chemicals. All chemicals were sourced from Sigma-Aldrich, unless otherwise stated, and were typically 99% pure or greater.

Construction of Expression Bacteria. Details of the creation of full-length murine PrP (amino acids 23−230) of the $prnp^{a}$ genotype with the proline to leucine mutation at amino acid 164 have previously been published (*11*). In the current work additional variants were constructed that incorporated serine, glutamine, or glutamic acid at codon 164. Mutants were constructed by site-directed mutagenesis (QuickChange II; Stratagene) using the full-length mouse PrP clone, the production of which has been described previously (*11*), as a template and the following primers: forward primer 5′-CCAAGTGTACTACAGGXXX-GTGGATCAGTACAGC-3′, where XXX corresponds to TCA, CAA, and GAA for serine, glutamine, and glutamic acid mutants, and reverse primer 5′-GCTGTACTGATCCACXX-XCCTGTAGTACACTTGG-3′, where XXX corresponds to TGA, TTG, and TTC for serine, glutamine, and glutamic acid mutants. Correctly mutated plasmids, as determined by sequencing, were transformed into Rosetta DE3 pLysS bacteria for protein expression.

Protein Production. The expression, purification, and refolding of recombinant prion proteins have already been described elsewhere (*12*). Briefly, bacteria were grown to an OD_{600} of 0.6−1.0, and protein expression was induced by the addition 1 M isopropyl β-D-1-thiogalactopyranoside (IPTG) to a final concentration of 1 mM. Bacteria were cultured further overnight and harvested by centrifugation. The cell pellet was resuspended in 50 mM Tris-HCl, pH 8.0, containing 1 mM EDTA and 100 mM NaCl. Bacteria were lysed by the addition of lysozyme (final concentration 200 μg/mL) followed by addition of sodium deoxycholate (final concentration 1 mg/mL) and DNase (final concentration 10 μg/mL). Protein-containing inclusion bodies were harvested by centrifugation and were then solubilized in a buffer containing 8 M urea, 100 mM Na_2HPO_4, and 10 mM Tris, pH 8.0. For conversion assays and circular dichroism (CD) analyses, protein was purified by binding to a column of immobilized nickel ions (Ni-IMAC; Qiagen), eluting bound proteins by step elution to pH 4.5. The protein was further purified by cation-exchange chromatography (SP-Sepharose; GE Healthcare), eluting bound components with a gradient from 0 to 500 mM NaCl. PrP-containing fractions were pooled and diluted to a concentration of approximately 0.1 mg/mL, and a 5-fold molar excess of Cu^{2+} ions was added, overnight, to oxidize the disulfide bond. The final protein was dialyzed extensively against 50 mM sodium acetate, pH 5.5, and was finally concentrated to 0.5−1.0 mg/mL for use. For all experiments repeats using different batches of proteins were used.

Cell-Free Conversion Assays. Details of our cell-free conversion assay have previously been published (*11*, *12*). Briefly, recombinant proteins were produced as above, except bacteria were grown in M63 minimal media supplemented with [^{35}S]methionine during induction of protein expression. This yielded radiolabeled recombinant protein, which was mixed with a seed of fibrils purified from the brains of terminally TSE-infected mice, by a procedure involving detergent extraction and differential centrifugation. The mixture of proteins was incubated at 37 °C for 24 h and was subsequently treated with proteinase K (PK), after prior removal of an aliquot equal to $^{1}/_{20}$th of the reaction mixture for use as a −PK control. All samples were separated by SDS−PAGE, and PK-resistant recombinant PrP was detected by autoradiography. The resulting autoradiographs were scanned by use of an ImageScanner III (GE Healthcare) and protein bands quantified by densitometric methods using ImageQuant software (GE Healthcare). Finally, for each set of paired samples, we set the densitometric intensity of the control sample (−PK) to 100% and calculated the percentage of protein left after PK treatment based on densitometric intensity.

Circular Dichroism and Thermal Denaturation of Protein Variants. All circular dichroism measurements were made by use of a Jasco J-710 spectropolarimeter. For standard CD

measurements a cell of path length 0.2 mm was used, and scans between 260 and 190 nm were acquired. At least 20 scans were summed with a scan rate of 100 nm/min and instrument response time of 4 s. For thermal denaturation experiments, protein samples were diluted to 0.1 mg/mL by dilution in 50 mM sodium acetate, pH 5.5. CD instrumental parameters remained the same, except that scans were taken between 230 and 210 nm and 10 scans were accumulated per temperature point. A sealed cell of path length 2 mm was used, and the cell was placed in a holder attached to a recirculating water bath to allow the sample to be heated to known nominal temperatures. A range of temperatures between 20 and 80 °C was used, with temperature points closer together between 50 and 80 °C, which represented the thermal transition. The CD reading at 222 nm was extracted from each spectrum for each temperature. At least six individual experimental repeats were done for each protein variant.

Data were normalized to assess the percentage of protein molecules that were unfolded at each temperature. To do this, we allowed the lowest (most negative) 222 nm reading in each data set to be 0% unfolded and the highest (least negative) to be 100% unfolded. To each data series a sigmoidal curve of the form $x = M/(1 + r^{(a-T)})$ was fitted, where r is the rate of thermal denaturation in $°C^{-1}$, a is the midpoint of the transition, and T is the temperature. M represents the maximum unfolded percentage, which should be equal to 100; however, this variable reached values slightly higher than this for proteins that had not reached 100% unfolding by the top temperature tested, 80 °C. This process allowed the midpoint of each transition to be extrapolated even from data that appeared not to have reached 100% denaturation and yielded at least six independent assessments of thermal denaturation midpoints per protein variant. Data sets were compared using standard one- or two-sided Student's t tests with unequivalent variances. To produce Figure 4, individual assessments of percent unfolded at each temperature were averaged, and a single sigmoidal curve was fitted to the average data for each protein variant.

Oligomerization of Protein Variants. Bacterial production and purification of PrP followed the above procedure up to and including preparation of an inclusion body pellet. Subsequent steps followed those published by Rezaei et al. (*13*). The inclusion body pellet was suspended in a buffer containing 8 M urea, 100 mM sodium phosphate, and 20 mM Tris-HCl, pH 8, and was applied to a nickel−Sepharose column (chelating Sepharose Fast Flow; Pharmacia). The column was washed with several column volumes of the same buffer, and bound proteins were removed by step elution using a 1 M imidazole solution in 20 mM MOPS, pH 6. The protein was buffer-exchanged into 20 mM sodium citrate, pH 3.4, by means of a PD-10 desalting column (GE Healthcare). Final protein concentration was measured by absorbance at 280 nm (DU650 spectrometer; Beckman) using an extinction coefficient of 62280 M^{-1} cm^{-1}. Protein variants were diluted to nominal concentrations of 75 μM and were refolded to oligomeric forms by heating the samples at 45 °C (Heraeus 200 incubator) in a 20 mM sodium citrate, pH 3.4, buffer. Fractions of size 10 μL were taken at 15 min intervals and analyzed using size exclusion chromatography.

Size Exclusion Chromatography. All size exclusion separations were performed by use of an AKTA purifier HPLC (Pharmacia) operating with a TSKgelG4000SW_{xl} gel filtration column (300 mm × 7.8 mm i.d.; TOSOH Bioscience). The column was calibrated with standards of known molecular masses (molecular mass kit 29000−700000 Da; Sigma Aldrich). Before each oligomerization experiment the column was equilibrated with 10 volumes of running buffer (20 mM sodium citrate, pH 3.4) prior to injection of three test samples of normally folded recombinant PrP to occupy nonspecific binding sites. The flow rate was at 1 mL/min, and 10 μL injections were analyzed, monitoring protein elution by UV absorbance at 280 nm. SEC chromatograms were intergrated using Unicorn software.

Molecular Dynamics. Molecular dynamics simulations were carried out by use of the AMBER (version 7) suite of molecular dynamics programs (*14*). Molecular trajectories were analyzed using AMBER software or with VMD analysis software (*15*), and figures were built using MOLMOL (*16*). The NMR coordinates for murine PrP residues 123−225 (PDB code 1AG2) (*17*) were obtained from the Protein Data Bank, and the mutations P164 to Leu, Gln, Glu, or Ser were made using the Deep View PDB viewer (*18*). In all cases, the most stable conformer, as determined by Deep View, was selected. Starting structures were energy minimized and equilibrated *in silico* to 37 °C, and molecular dynamics was carried out at 37 °C for 10 ns for each structure. A Born approximation of implicit solvent was used (*19*) to expedite simulations while a simulation of 200 mM salt was included to maintain buffering. Coordinates were output every 10 ps during each simulation, and every structure was analyzed for root mean squared (rms) deviation from starting and mean structures, for hydrogen bonds, and for change in ϕ,ψ angles.

RESULTS

Results from our recent work have demonstrated that the amino acid expressed at PrP codon 164 is of crucial importance in determining susceptibility to TSE disease. The detailed molecular mechanism for this effect has yet to be established, but this site is in close proximity to an additional polymorphism (ovine codon 171, codon 167 in mouse numbering) known to dramatically affect disease susceptibility. It is also in the loop region of the prion protein, hypothesized to be intimately involved in the misfolding transition (*20*) and in binding to the putative species-specific chaperone protein X, which has been suggested to facilitate conversion (*21*). Figure 1 shows schematically the position of residues 164 and 167 in the three-dimensional structure of the murine prion protein. Of significant interest would be the replacement of Pro164 with other amino acids to assess whether it is the loss of the proline that accounts for enhanced resistance to conversion or, conversely, whether it is specifically the change to a leucine residue. We have noted that, in addition to the Pro to Leu change in sheep, the equivalent codon can also be polymorphic in other species. Goats can express glutamine instead of the wild-type proline (*22*), while red deer can express serine (*23*).

We used site-directed mutagenesis to create bacteria that express PrP from the pTrc vector containing the substitutions P164Q and P164S on a murine background to create proteins 164Q-PrP and 164S-PrP. We also created an additional variant, 164E-PrP, since this change results in the incorporation of an acidic amino acid at this site, which we reasoned may result in differential efficiency of conversion. Coupled with the wild-type murine protein (164P-PrP) and our 164L-PrP variant, we have five related proteins, which were expressed and purified by standard metal-ion affinity and ion-exchange chromatography steps, the details of which have previously been published (*12*, *24*, *25*). We confirmed correct expression and purity of each protein by HPLC−mass spectrometry and SDS−PAGE (data not shown). These proteins were used for structural and misfolding studies as detailed.

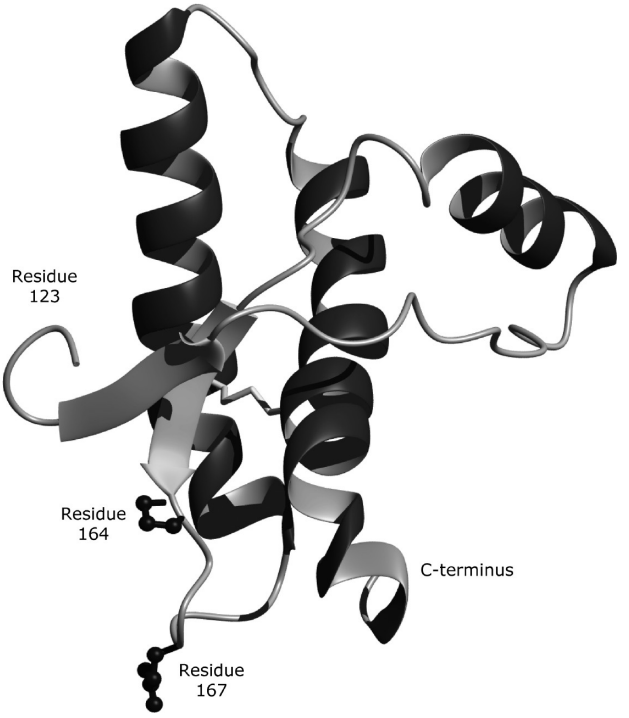

FIGURE 1: Schematic representation of the structure of murine PrP, residues 123−225, with highlighted residues Pro164 and Gln167 (equivalent to ovine Gln171). The structure was generated from PDB file 1AG2 and rendered by use of MolMol and PovRay for Windows.

Mutation at Residue 164 Does Not Dramatically Affect Overall Protein Tertiary Structure. After purification of protein variants, we investigated the effect that substitution of different amino acids at residue 164 had on the protein secondary structure. We acquired circular dichroism data for each of the protein variants, and typical CD spectra are shown in Figure 2. CD spectra of all full-length prion protein variants have minima at ~222 and ~208 nm, consistent with structures composed predominately of α-helix, indicating that our protein variants are correctly folded prior to experimentation. Small quantitative differences between CD spectra are the result of experimental errors in protein concentration estimations, and our data indicate that different substitutions at residue 164 do not greatly affect the overall secondary structure of PrP at ambient temperatures.

Cell-Free Conversion Assays Reveal Dramatically Different Conversion Efficiencies of Protein Variants. Cultures of each type of bacteria were grown in M63 minimal media, and after induction, addition of [^{35}S]methionine to the growth media produced radiolabeled, recombinant PrP proteins. The proteins were purified and refolded, and the conversion efficiency of each protein was assessed by use of our cell-free conversion assay. Briefly, our *in vitro* conversion assay uses a seed of PrP^{Sc} fibrils isolated from the brains of terminally sick, TSE-infected animals as a catalyst to convert recombinant protein to a protease-resistant isoform. In the current experiments, we used fibrils purified from mice infected with the 87V strain of scrapie as a seed, and each assay was performed in triplicate. At least two repeat assays were done for each protein variant yielding a total of at least six replicates for each assay. The products of the conversion assay were treated with proteinase K, proteins were resolved by SDS−PAGE, and protein bands were detected by autoradiography.

Figure 3a shows a standard result from conversion of 164P-PrP protein by 87V fibrils. In the absence of fibrils, no PK-resistant recombinant PrP is produced (lane 2, panel a); however, when the recombinant protein is incubated in the presence of fibrils, a PK-resistant product can be detected (lane 4, panel a). Panels b and c of Figure 3 show equivalent autoradiographs for conversion assays with 164E-PrP and 164Q-PrP protein. For these CFCA reactions, a PK-resistant product can be detected; however, the abundance of these products is markedly reduced compared to those generated from wild-type proteins. Conversely, Figure 3d shows the CFCA with 164S-PrP as substrate, which demonstrates that conversion efficiency of the protein is restored to similar levels to the wild-type 164P-PrP variant.

Results from all assays were quantified by means of densitometry, and data were normalized to calculate the percentage of the starting material that had been converted in each case. The results are shown graphically in Figure 3e. In these assays, the 164P-PrP variant converts with an average efficiency of ~3.5% while 164Q-PrP and 164E-PrP protein variants have reduced conversion efficiencies of ~0.5% and ~1%, respectively. The 164S-PrP protein variant converts at similar levels to 164P-PrP. We analyzed the data using a two-tailed Student's t test assuming unequal variances. We find that the reduction in conversion efficiency for 164Q-PrP and 164E-PrP, relative to both 164P-PrP and 164S-PrP, is statistically significant ($p < 0.01$), while the conversion efficiencies of 164Q-PrP and 164E-PrP are not significantly different from each other. Equally, we find no statistical difference between conversion efficiencies of the 164P-PrP and the 164S-PrP variants.

Protein Variants That Convert Inefficiently Are Structurally More Thermally Labile Than Those That Convert Efficiently. The efficiency with which proteins convert in the CFCA has previously been shown to reflect the effect of protein variants on disease susceptibility *in vivo*. This property of protein variants may be intrinsically linked to stability; therefore, we assessed whether our proteins containing mutations were more or less stable to thermal denaturation than the wild-type protein, 164P-PrP. We used circular dichroism to determine the ellipticity at 222 nm, corresponding to the peak signal for α-helix, as a function of temperature for each protein variant. All protein variants were diluted to give a nominal concentration of 0.1 mg/mL, but the data were also normalized to range from 0% to 100% unfolded to correct for minor variations in protein concentration. Sigmoidal curves were fitted to the data, using a least-squares approach, by allowing variables associated with denaturation rate, onset, and midpoint to adopt suitable values, and this process allowed transition midpoints to be calculated for each data set acquired. We generated at least six replicate sets of data for each protein variant and compared thermal denaturation midpoints using a two-tailed Student's t test.

Averaged thermal denaturation data are shown in Figure 4, and denaturation rates, as a function of temperature, are similar for 164P-PrP, 164L-PrP, 164Q-PrP, and 164S-PrP variants. However, the denaturation curves for the variants 164Q-PrP and 164L-PrP are shifted to lower temperatures relative to that for the 164P-PrP variant. These data demonstrate conclusively that proteins containing the amino acid substitutions 164L and 164Q are significantly less stable ($p < 0.01$) than either 164P-PrP or 164S-PrP. In addition, 164L-PrP is less stable than 164Q-PrP ($p < 0.001$). There was no significant difference between the stability of the 164P-PrP and the 164S-PrP variants, and full t test results are reported in Table 1. Thus, the thermal stability of proteins correlates with TSE-specific conversion efficiency, as judged by our cell-free conversion assays, indicating that those proteins most susceptible to conversion are also the most

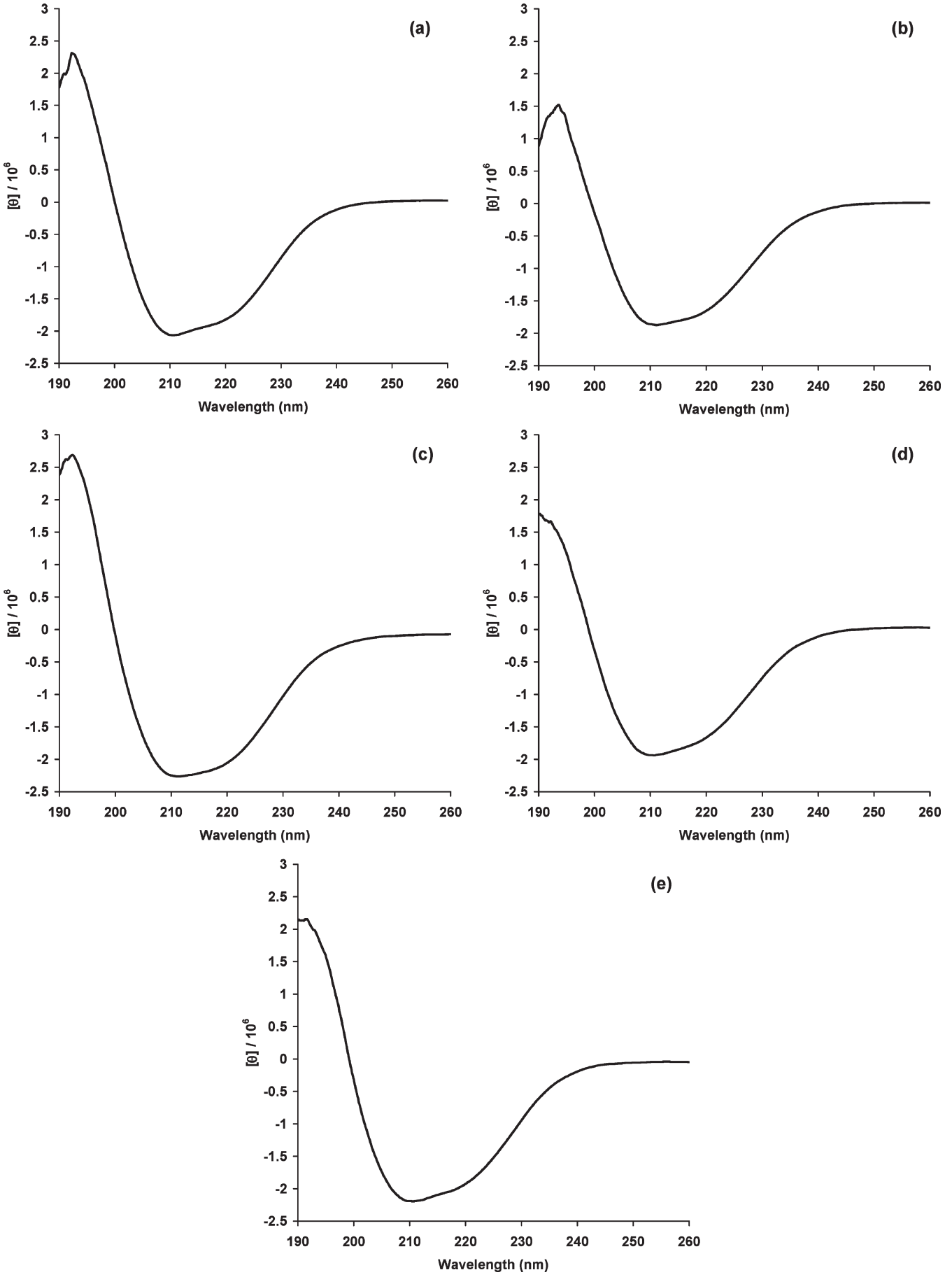

FIGURE 2: Far-UV circular dichroism spectra of α-helically folded PrP: (a) 164P-PrP, (b) 164L-PrP, (c) 164Q-PrP, (d) 164E-PrP, and (e) 164S-PrP proteins. Protein samples were ~1 mg/mL, and a cell of path length 0.2 mm was used. Raw CD data were transformed to molar elipticities for comparison. The units of molar ellipticity [θ] are deg cm^2/mol.

thermally stable. This result is the opposite to what may be expected, since one would intuitively expect proteins that convert efficiently to protease-resistant isoforms in seeded assays to be less stable than those that do not.

We also performed thermal denaturation studies on 164E-PrP, and the averaged denaturation data are also plotted graphically on Figure 4. This protein variant has a reproducibly more rapidy rate of thermal denaturation than the other protein variants studied, which yields a lower midpoint of denaturation. However, the difference in the rate of thermal denaturation, relative to the other variants, is indicative of a different mechanism of unfolding of this protein. This is under investigation within our laboratory, and since we do not think it is valid to compare denaturation profiles of proteins that appear to unfold by different mechanisms, we have not calculated whether the midpoints of the curves for the 164E-PrP protein are statistically different from the other proteins studied.

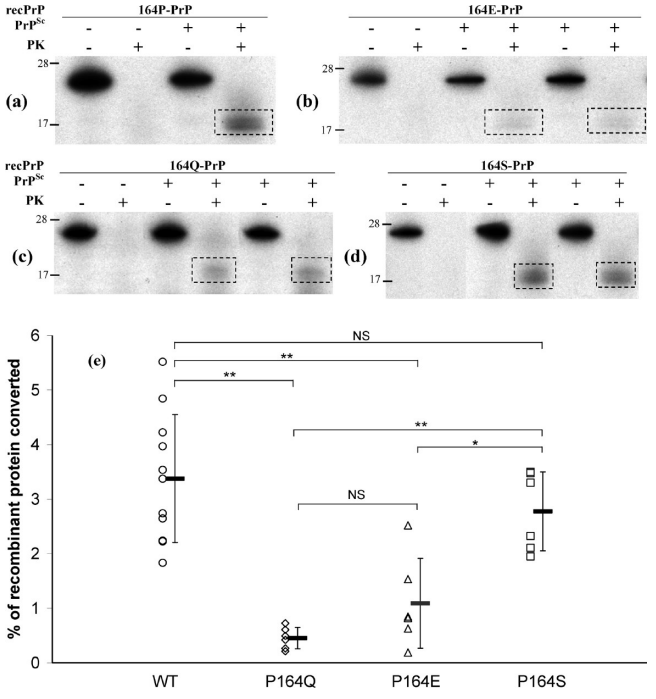

FIGURE 3: Cell-free conversion assays of protein variants. Proteins were incubated in the presence or absence of PrP^{Sc} seed, and PK-resistant products were detected by SDS−PAGE and autoradiography. (a) 164P-PrP, (b) 164E-PrP, (c) 164Q-PrP, and (d) 164S-PrP. All assays were performed at least six times, and densitometric analysis of PK-resistant bands yielded conversion efficiency, relative to non-PK-treated control bands. (e) Graphical representation of data from replicate conversion assay experiments, showing individual conversion efficiencies (open symbols) and the mean conversion efficiency ± standard deviation. Student's *t* tests were performed to determine statistical significance of differences in conversion efficiencies. ** = $p < 0.001$; * = $p < 0.01$; NS = not significant.

Thermal Lability of Proteins Correlates with Tendency To Misfold to Oligomeric Isoforms. Next we assessed whether the thermal lability of protein variants affected the intrinsic ability of the prion protein to misfold. In the absence of a PrP^{Sc} seed, recPrP can be induced to misfold into various isoforms that mimic PrP^{Sc}. We investigated whether there were differences in rates of unseeded, *in vitro* oligomerization as a function of the amino acid expressed at codon 164. Since we had already established that there were differences in thermal stability between proteins, we chose a method of oligomerization mediated by elevated temperatures at low pH to induce oligomerization (*26*)

Table 1: Student's *t* Tests To Evaluate the Significance between Thermal Denaturation Data for Protein Variants[a]

	Two tailed Student's t-test			
	164P-PrP	**164S-PrP**	**164Q-PrP**	**164L-PrP**
164P-PrP		0.50	0.0017	< 0.001
164S-PrP			0.0069	< 0.001
164Q-PrP				< 0.001
164L-PrP				

[a]Thermal denaturation data were acquired for each protein variant on a minimum of six separate occasions and sigmoidal curves fitted to individual data sets. *P* values represent the probability of the set of curve midpoints for each data set being derived from the same overall set.

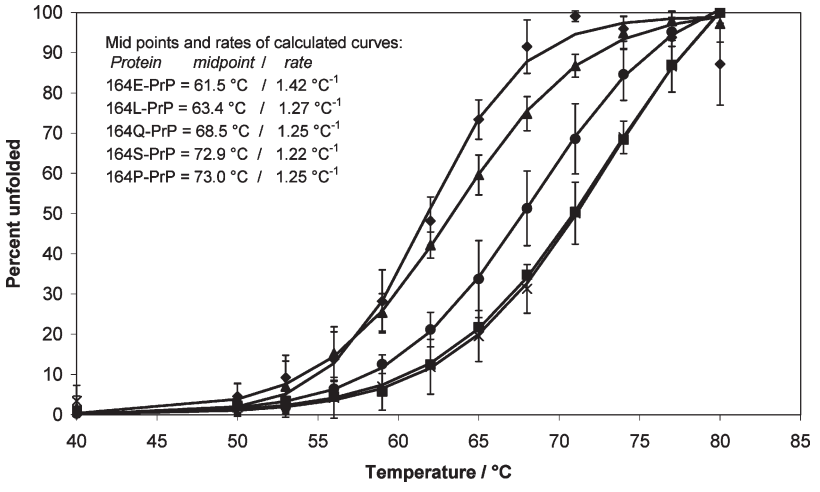

FIGURE 4: Thermal denaturation of protein variants. Protein samples at ~0.1 mg/mL were monitored by circular dichroism at 222 nm as the temperature of the sample was gradually increased by means of a circulating water bath. The data were normalized to give a transition between 0% and 100% unfolded, and sigmoidal curves were fitted to the data (see Materials and Methods) from which midpoints of the transitions were calculated. The data represent the average of at least six independent replicate experiments for each protein variant. Key: (×)164P-PrP; (●) 164Q-PrP; (▲) 164L-PrP; (◆) 164E-PrP; (■) 164S-PrP.

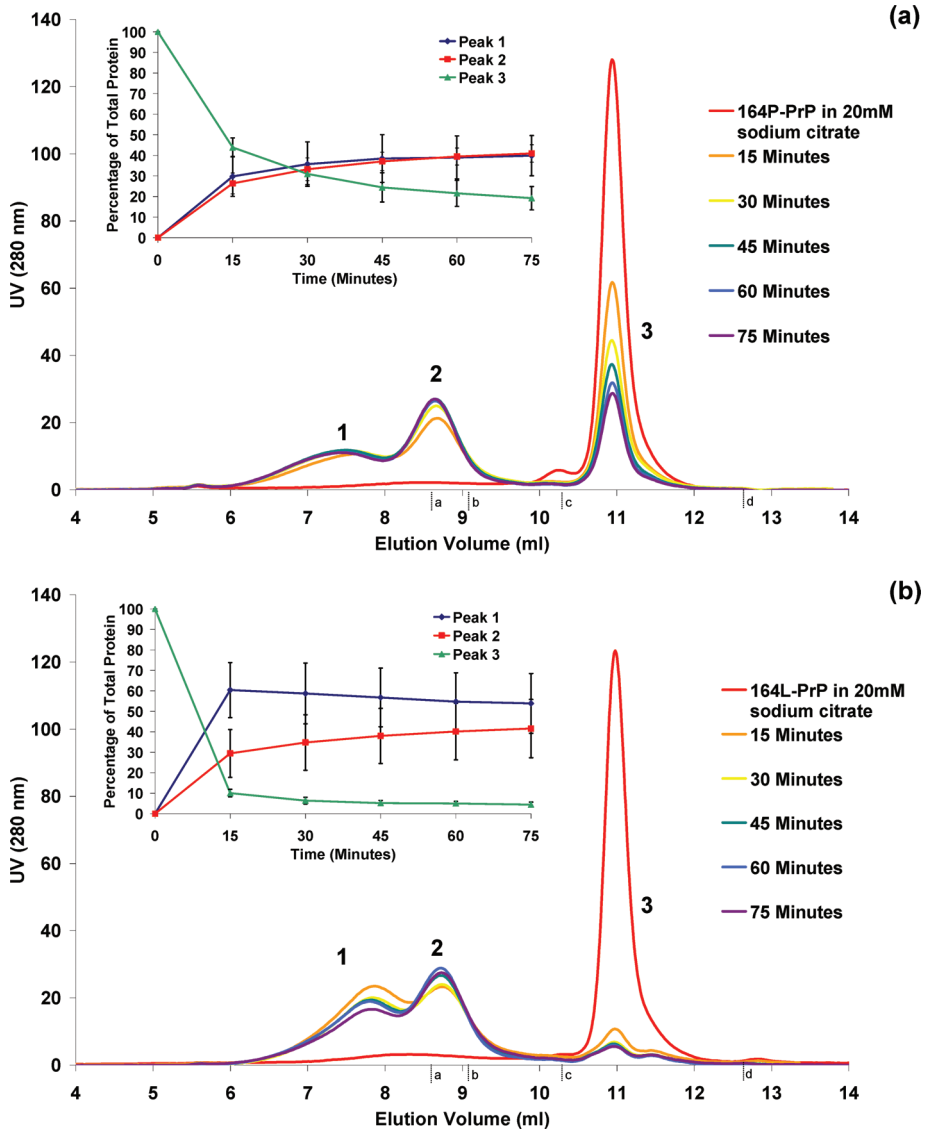

FIGURE 5: Size exclusion chromatography analysis of oligomerization of (a) 164P-PrP and (b) 164L-PrP. Proteins were incubated at 45 °C in oligomerization buffer, and aliquots were withdrawn every 15 min for SEC analysis. The starting material is largely monomeric (peak 3) while two different oligomeric species are produced during the oligomerization reaction (peaks 2 and 1). Insets: Experiments were repeated three times for each protein variant and the chromatograms integrated to yield the percentage of total protein contained within each peak. The data are plotted against oligomerization time. Calibration points for the SEC column are shown on the *x*-axis and relate to data from (a) thyroglobulin, 660 kDa, (b) apoferritin, 443 kDa, (c) γ-globulin, 150 kDa, and (d) *p*-aminobenzoic acid, 137 Da.

and focused on the 164P-PrP and 164L-PrP proteins to represent the two extremes of thermal stability. This oligomerization technique has been used previously by Rezaei et al. to demonstrate correlations between oligomerization and misfolding.

Proteins were incubated in a buffer of sodium citrate, pH 3.4, at 45 °C, and aliquots were taken at various time intervals. The extent of oligomerization was assessed by size exclusion chromatography, and representative chromatograms for both wild-type and 164L-PrP proteins are shown in Figure 5. In all cases, three peaks are present in the SEC chromatograms and are labeled according to the nomenclature developed by Rezaei et al. (*26*). P3 represents the monomeric protein, P2 corresponds to a small oligomer, previously estimated from small-angle X-ray scattering to consist of 12 molecules of PrP, and P1 corresponds to a large oligomer, believed to consist of 36 molecules. Retention volumes of the peaks were consistent across all repeat experiments and averaged ~11 mL for P3, 8.8 mL for P2, and 7.9 mL for P1. Furthermore, we collected fractions of each peak and confirmed that they were caused by recPrP eluting from the SEC column by silver-stained SDS−PAGE analysis (data not shown). Figure 5a shows representative SEC chromatograms from the oligomerization of wild-type murine protein. Over time, the monomeric protein (P3) is lost to produce increasing amounts of both of the larger oligomeric isoforms P2 and P1. Conversely, SEC analysis of oligomerization of the 164L-PrP variant (Figure 5b) shows immediate loss of monomeric protein to produce both oligomeric isoforms P2 and P1, but over the course of the oligomerization, the large oligomer P1 appears to be lost to form P2. Thus, the two protein variants appear to have somewhat different time courses of oligomerization, but the most striking observation is the complete loss of monomeric 164L-PrP protein at the earliest time point study.

The experiments were repeated three times for each protein, and the percentage of each species, as a function of total protein, was calculated by integrating SEC chromatograms for each time point. Averaged data for wild-type and 164L-PrP proteins are

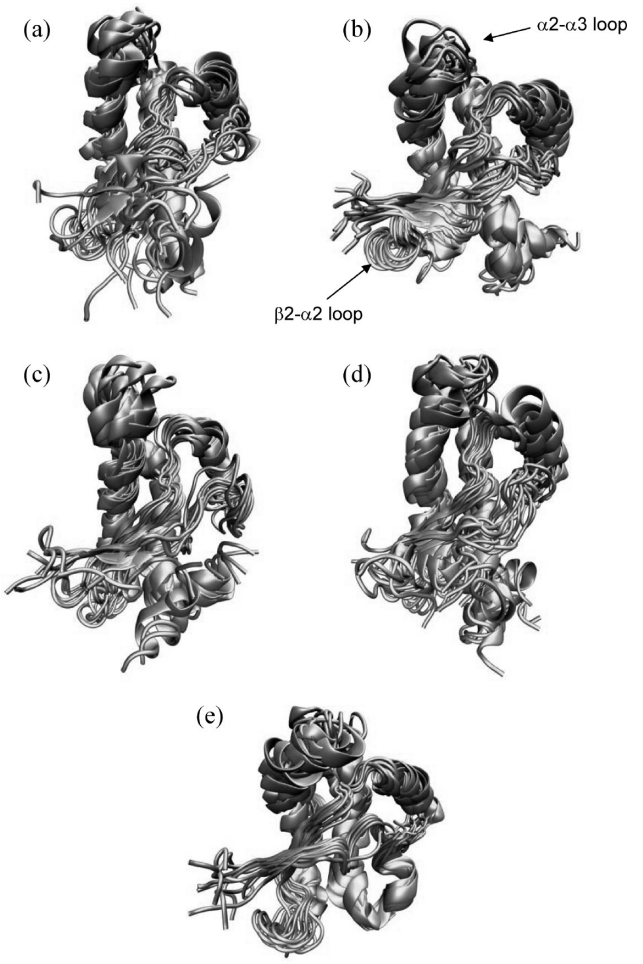

FIGURE 6: Overlay of structures from every 1 ns of molecular dynamics simulation of (a) 164P-PrP, (b) 164L-PrP, (c) 164Q-PrP, (d) 164E-PrP, and (e) 164S-PrP. Structures were rotated to fit to the starting structure to remove artifacts caused by rotational and translational motion. Each structure is the average of structures output for the 100 ps preceding and following the 1 ns time point during the calculations.

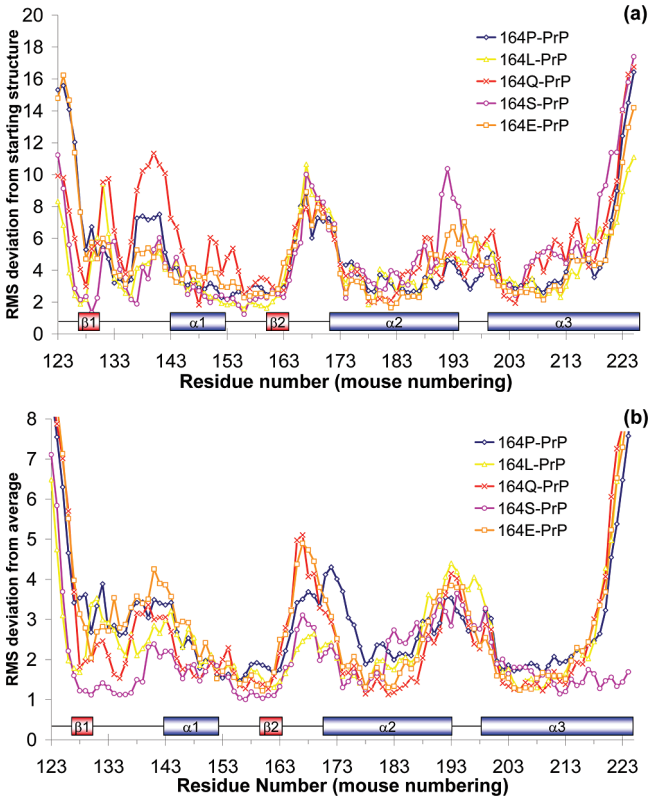

FIGURE 7: Root mean squared deviations of individual residues from either (a) the starting structure or (b) the average structure during molecular dynamics simulations of the five protein variants. Deviations were calculated based on movement in backbone heavy atoms (amide nitrogen, α-carbon, carbonyl carbon, and carbonyl oxygen) from structures output every 10 ps during the course of the molecular dynamics simulations.

shown graphically in the insets of Figure 5. Comparison of panels a and b of Figure 5 clearly demonstrates the increased propensity of the 164L variant to unfold relative to wild-type protein, presumably to produce large, P1, oligomers. However, the production of P2 oligomers is roughly equal for wild-type and 164L-PrP proteins. Thus, in line with our thermal denaturation data, we find that the 164L protein variant forms oligomers significantly more rapidly than the wild-type protein, implying that structural lability correlates with a greater propensity to generically misfold.

Molecular Dynamics Simulations Suggest Similar Peptide Backbone Mobility for Each Protein Variant. To explore the reasons for the dramatic differences between the misfolding behavior and structural stability of our protein variants, we have applied molecular dynamics simulations to each of the five protein variants. These simulations enable atomic level descriptions of the potential noncovalent bonding within each protein and hence suggest conformational variations that may cause differences in thermal stability. Starting with coordinates for residues 123−225 of wild-type murine PrP (PDB code 1AG2 (*17*)), we used Deep View Swiss PDB Viewer (*18*) to make mutations at codon 164 and saved the resulting coordinates as PDB files. The AMBER suite of programs was used to perform MD simulations (*14*). First, each structure was energy minimized to remove local "hot spots" introduced by the amino acid changes, and then the structures were raised to an *in silico* temperature of 310 K (equivalent to 37 °C) and equilibrated for 5 ps. MD was performed over 10 ns for each structure, and coordinates were output every 10 ps for analysis.

Figure 6 shows an overlay of structures output every 1 ns over the course of the simulations for each protein variant. For each protein variant there is significant movement during the simulations in the loop region around the polymorphic amino acid as well as in the loop region between helices 2 and 3. Motion in these regions is in line with other MD simulations of prion proteins at physiological pH. In none of the cases was extensive helical unwinding nor increased β-sheet formation observed. Thus, at a gross structural level, molecular dynamics simulations do not suggest reasons for reduced thermal stability and increased rates of oligomerization of 164L-PrP, 164Q-PrP, or 164E-PrP variants relative to 164P-PrP or 164S-PrP variants.

To analyze motion in the protein backbone in more detail, we calculated root mean squared (rms) deviations of the heavy backbone atoms (amide nitrogen, α-carbon, carbonyl carbon, and carbonyl oxygen) from both the starting structures and the average structures for each of the variants, and Figure 7 shows the results of these analyses plotted graphically against residue number. Rms deviations are largest in loop regions, while helical sections of secondary structure remain largely immobile during simulations. These results are in line with those already in the literature for MD simulations of PrP. In our study, while there are some local differences in the rms deviations from the starting

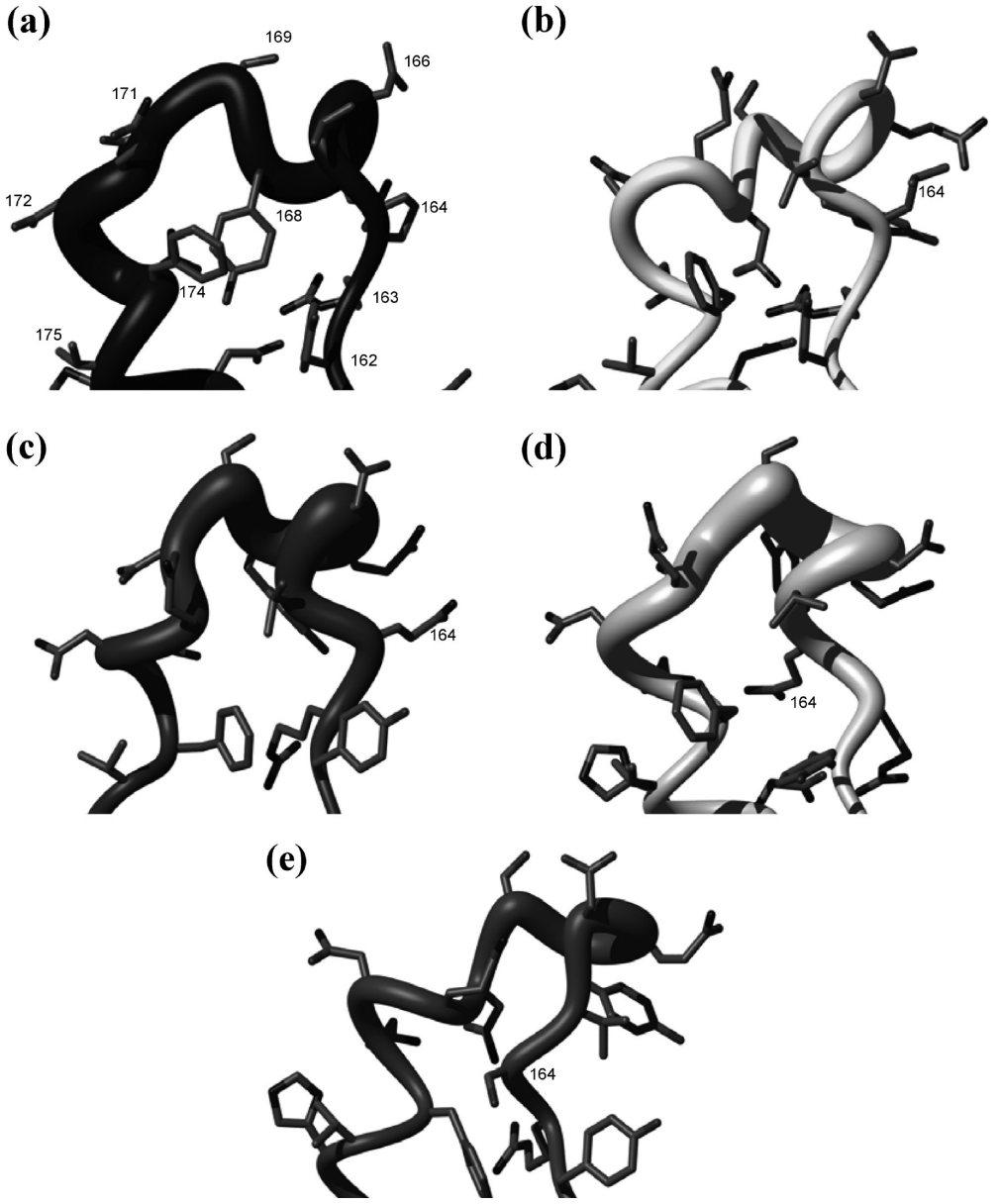

FIGURE 8: Schematic representation of the $\beta2-\alpha2$ loop region of the average structures calculated for (a) 164P-PrP, (b) 164L-PrP, (c) 164Q-PrP, (d) 164E-PrP, and (e) 164S-PrP. The width of the spline is proportional to the rms deviation of all structures from the average structure for each residue. All structures were aligned to the wild-type structure to show equivalent areas of structure. The portion of the protein shown comprises Y_{162}R*VDQYSNQNNFV, where the asterisk represents the mutated amino acid corresponding to P, L, Q, E, and S, respectively.

structures, no regions of PrP had rms deviations that were dramatically different for any of the protein variants studied.

Averaged Structures from MD Simulations Reveal That Subtle Conformational Differences in PrP^C *May Underlie Variations in Structural Lability*. Finally, we wanted to assess whether alteration of the residue expressed at codon 164 changed the secondary structure in the $\beta2-\alpha2$ loop region of the protein, the region that is directly adjacent to the polymorphic site. Previous experimental and theoretical studies have indicated that a single amino acid change in this region can dramatically affect local conformation. We calculated average structures across the course of each molecular dynamics simulation and compared the five structures generated. There was substantial overlap between all structures in many secondary structural elements; however, when we compared the loop region of each structure in isolation, we found subtle differences between them. Schematic representations of the averaged structures adopted by the loop region of each of the proteins are shown in Figure 8. For each protein, the diameter of the spline is proportional to the rms deviation of the backbone atoms of each amino acid, to give an indication of the "error" associated with the average structures calculated. Also highlighted on these figures, for each structure, are the side chains of amino acids in this region.

All average structures show differences in the atomic level structures calculated. For example, while the 3_{10} helix, between residues 164 and 168, in the loop region of wild-type mouse PrP is retained in 164L-PrP, 164Q-PrP, and 164E-PrP variants, it is at least partially absent in the averaged structure of the 164S-PrP variant. This leads to (or, more likely, is a result of) reduced solvent accessibility of residue 164, the side chain of which points into the molecule and makes hydrogen bonds with residues in helix 3 through the hydroxyl hydrogen. These interactions may help to stabilize the structure. In addition, the side chain of Glu164 in the 164E-PrP variant points largely into the inner part

of the molecule making contacts across the loop with residues 168−170. This leads to displacement of the side chain of Arg163 from the interloop region, and the substantial variation in charge that will result suggests a potential reason for the accelerated rate of thermal denaturation of this variant.

The mutation of codon 164 from a proline to any other amino acid creates additional functionality, since proline residues lack an amide hydrogen for hydrogen bonding. Thus, the substitutions 164L, 164Q, 164E, and 164S all produce additional amide backbone hydrogen atoms capable of hydrogen bonding. In the structures of the 164L-PrP and 164Q-PrP, which are thermally labile and resistant to conversion, the extra atom is involved in hydrogen bonds to carbonyls in the N-terminal region of the structure, specifically residue 127, in 89% and 39%, respectively, of the structures output during MD simulations. This residue is at the N-terminal side of the first section of β-sheet, and these hydrogen bonds may facilitate the elongation of β-strands in the thermally labile proteins. The hydrogen bond is present in less than 2% of the structures of the 164S-PrP variant and is obviously absent from the wild-type structures. In 164E-PrP, the extra amide hydrogen is involved in hydrogen bonds with the side chain of amino acid Asp177; this is the only variant in which this hydrogen bond is present, and this may also explain the apparently different mechanism of unfolding. Thus, our averaged structures from molecular dynamics simulations suggest that the loop regions of each protein adopt different conformations that could explain the thermal lability of 164L-PrP, 164Q-PrP, and 164E-PrP variants relative to 164S-PrP and 164P-PrP proteins.

DISCUSSION

This paper details work addressing the mechanism by which susceptibility to TSEs can be mediated through the amino acid expressed at codon 164. This residue occurs at the end of the second β-strand and within the $\beta2-\alpha2$ loop region of the protein. This loop region also contains Gln167 (equivalent to ovine residue 171), which is known to modulate disease susceptibility in sheep, and the importance of the $\beta2-\alpha2$ loop (residues 165−173) in TSE disease has been highlighted recently in a number of publications. Agrimi et al. found that the amino acid difference at residue 169 between mice and voles (mice express serine at codon 169 while voles express asparagine) was at least partially responsible for the differential susceptibility of these species to both scrapie and BSE (*27*). Elk also express asparagine at codon 169, and by use of molecular dynamics, Gorfe et al. showed that the amino acid incorporated at codon 169 critically controlled the conformational freedom of the loop region (*28*). Furthermore, Sigurdson et al. produced transgenic mice in which the loop region was "cervidized", by creating the mutations Ser169Asn and Asn173Thr, resulting in spontaneous TSE disease with 100% attack rate (*29*). Thus, the loop region of PrP is of critical importance in different species and may exert primary control over susceptibility to TSEs.

Previously, we identified codon 164 of PrP as a site that is critically involved in the modulation of protein conversion and, hence, disease susceptibility across two species and with two different sources of TSE disease (*11*). That work focused on the substitution Pro-Leu at codon 164, since the equivalent mutation was found in a number of sheep experimentally infected with BSE (*10*); the mutation conferred dramatically increased resistance to disease in these animals. In the current work, we have extended our investigations into the mechanisms of codon 164 polymorphism-mediated resistance by creating and analyzing protein variants incorporating Pro-Gln, Pro-Ser, and Pro-Glu substitutions. We have used a powerful combination of four different *in vitro* and *in silico* approaches to shed light on mechanisms of protein misfolding. Our initial experiments indicated that all protein variants adopted similar secondary structures after *in vitro* refolding, despite the presence of five different amino acids with different biophysical properties.

By use of cell-free conversion assays of each variant, we demonstrated that the wild-type murine protein converted to a PK-resistant isoform efficiently, and we have previously published data demonstrating that the 164L variant converted with low efficiency (*11*). In the current work we also found that the Pro-Gln and Pro-Glu substitutions produced proteins resistant to conversion, while the 164S-PrP variant converted with efficiencies similar to those of the wild-type protein. Thus, we have identified two novel PrP alleles that we predict to be highly resistant to conversion and, therefore, that would confer disease resistance on animals in which they are expressed. Interestingly, the P164Q polymorphism has been identified in goats, and our findings highlight the possibility of breeding for this polymorphism as a means of increasing TSE resistance in this species. This may be of considerable future importance given the recent finding of goats infected with BSE in Europe (*30*).

Coupled with our previously published results showing resistance of 164L-PrP to conversion, our CFCA results for 164Q-PrP and 164E-PrP indicate that it is not specifically the incorporation of leucine at residue 164 that confers resistance. Additionally, the fact that the 164S-PrP converts to a protease-resistant isoform with efficiencies similar to wild-type levels indicates that the presence of a proline residue in this location is not crucial for efficient conversion. These results greatly facilitate the search for mechanism, since we have now identified two related proteins that convert efficiently in our CFCA assay and three proteins that appear to be resistant to conversion. Our CFCA has been shown to mimic many aspects of *in vivo* disease and, for at least certain mechanistic investigations, is of significantly more utility than PrP-res amplification systems, such as the protein misfolding cyclic amplification (PMCA) technique (*31*), since our assays use only enriched or purified components. We purify the recombinant PrP substrate by biochemical methods and so can produce protein that is >95% pure. We also purify scrapie-associated fibrils (SAFs) by detergent extraction and differential centrifugation; while we know that these preparations are not 100% pure, the resulting CFCA system is still more defined than *in vivo* or *in* vitro amplification experiments. This allows us to put limits on the possible mechanisms of modulation of conversion, since complex cellular pathways cannot be involved. While we cannot rule out the involvement of additional molecules present in the PrP^{Sc} seed, our data indicate that codon 164-mediated resistance is likely to be modulated by differential stability of PrP^{C}, differential stability of the novel PrP-res formed from the different variants, or the ability of different protein variants to interact with the exogenous PrP^{Sc} seed.

We tested the possibility that alterations at residue 164 affect the stability of PrP^{C} by assessing the thermal denaturation profiles of each of our variants. Interestingly, we found that melting temperatures of our protein variants were significantly different, depending on the amino acid incorporated at residue 164. Crucially, we also found a positive correlation between protein stability and CFCA conversion efficiency. The two proteins that converted efficiently in the CFCA were significantly more thermally stable than those that did not. While this result

may seem counterintuitive, it is in line with findings of other researchers who have investigated the stability of prion protein carrying other TSE susceptibility-related polymorphisms. For instance, the ovine $V_{136}R_{154}Q_{171}$ (ovine numbering) PrP allotype is associated with susceptibility to scrapie and is significantly more thermodynamically stable than the ARR allotype, which is associated with resistance to classical sheep scrapie (*32*−*34*). The different proteins also appear to undergo somewhat different unfolding transitions resulting in different misfolding intermediates (*35*, *36*). It has been suggested that the properties of these proteins may result in the ARR protein misfolding generically more readily *in vivo* than the VRQ protein, which stimulates its clearance by cellular quality control machinery. The net effect would be a reduction in the half-life of the ARR protein, relative to the VRQ protein, and a corresponding reduction in the apparent substrate for conversion by PrP^{Sc} during TSE disease. This hypothesis is difficult to test *in vivo*, but additional evidence for enhanced clearance of resistance-associated proteins comes from various indirect methods. Immunoassays of PrP^{Sc} deposition in clinically affected sheep found reduced levels of PrP^{Sc} in animals that were more resistant to infection (as judged by longer incubation times) (*37*) while recombinant ovine prion protein variants inoculated intravenously into healthy sheep resulted in enhanced clearance of the ARR recombinant protein relative to the VRQ allotype (*38*).

In order to test whether the reduced thermal stability of our 164 variants was associated with an increased tendency to generically misfold, we carried out oligomerization assays using wild-type murine PrP and the 164L-PrP variant. We focused on these two proteins since they represent two extremes of thermal stability for the proteins studied. We have previously made use of *in vitro* misfolding assays to investigate the folding landscapes of various prion proteins (*39*−*41*). Previously, we used a method of oligomerization based upon chemical denaturation of the prion protein to demonstrate that oligomerization of human proteins occurs more rapidly when the protein is of the Met129 allotype than when it is the Val129 allotype (*41*), and it has recently been found that prion protein oligomers are toxic *in vitro* and *in vivo* (*42*). Our current oligomerization data indicate a significantly increased rate of oligomerization for the resistance-associated 164L-PrP variant, relative to 164P-PrP, presumably as a direct result of the reduced thermal stability of this variant. The assay takes place without preformed seed of either PrP^{Sc} or oligomer and, therefore, further restricts the mechanistic possibilities for differential susceptibility to conversion to those that do not involve PrP^{Sc}. The data provide strong additional evidence for an enhanced ability of thermally labile proteins to generically misfold relative to thermally stable prion variants.

To attempt to decipher an atomic level rationale for the reduced thermal stability of 164L-PrP, 164Q-PrP, and 164E-PrP relative to 164P-PrP and 164S-PrP, we performed detailed molecular dynamics simulations. At a molecular level these simulations did not predict extensive unfolding of any variant, within the time scale of the simulations. However, on close inspection of the $\beta2-\alpha2$ loop regions of the five protein variants, significant differences in mobility, average structure, and hydrogen bonding could be detected. In particular, differences could be detected in the way that the extra amide hydrogen, created by replacement of Pro164, bonds in the different molecules. In structurally stable proteins, the amide hydrogen is either absent (164P-PrP) or is not involved in hydrogen bonding (164S-PrP). However, in thermally more labile proteins, this amide hydrogen bonds either to more N-terminal residues (164L-PrP and 164Q-PrP), potentially leading to elongation of β-strands, or across the loop region (164E-PrP). This latter observation creates a completely different charge environment within the $\beta2-\alpha2$ loop in 164E-PrP and may explain the different unfolding transition observed for this protein. Interestingly, we have performed equivalent molecular dynamics simulations for all possible 164 variants of PrP and find hydrogen bonding between the extra amide hydrogen of residue 164 and N-terminal residues in around half of the protein variants. These data will be published separately, but this indicates that the creation of alternate variants of PrP differing at codon 164 may produce additional molecules in which we can test whether differential hydrogen bonding in this region does promote thermal lability.

Although the above discussion leads to a hypothesis that resistant-associated proteins may generically misfold more rapidly leading to enhanced clearance by cellular machinery, this argument cannot be applied to our cell-free conversion assay, in which intact cells are absent. The assay produces results that appear to agree with *in vivo* data, at least for sheep expressing the 164L-PrP variant, and we assume that it also recapitulates disease susceptibility for animals expressing the other variants for which biological data do not exist. It is known that a correctly folded substrate is an important prerequisite for efficient conversion in the cell-free conversion assay (*43*), and prion protein variants that generically misfold more readily may therefore be poor substrates for CFCA as well as being turned over *in vivo* more rapidly. The hypothesis of enhanced clearance *in vivo* remains difficult to test and is partially dependent on the ability to detect and quantify alternately misfolded forms of PrP either *ex vivo* or, more usefully, *in vivo*. This is a significant problem in general in the field of protein misfolding diseases, since there is a dearth of reagents recognizing specific, multimeric structures. The ability to distinguish oligomeric, fibrillar, aggregated, and normal forms of a single protein would provide a major leap forward in this field. In the meantime, our results strengthen the case for TSE resistance mediated by enhanced clearance. If proven, this hypothesis would also have profound implications for the search for therapeutic compounds to ameliorate TSE pathogenesis; our results suggest that compounds which stabilize the structure of PrP^{C} would have a detrimental effect on TSE disease.

ACKNOWLEDGMENT

We thank Abdou Tahiri-Alaoui for help leading to development of the oligomerization assay and Teresa Pinheiro for useful discussions and supervision of J.F.G.

REFERENCES

1. Aguzzi, A., Sigurdson, C., and Heikenwaelder, M. (2008) Molecular mechanisms of prion pathogenesis. *Annu. Rev. Pathol. 3*, 11–40.
2. Pan, K. M., Baldwin, M., Nguyen, J., Gasset, M., Serban, A., Groth, D., Mehlhorn, I., Huang, Z. W., Fletterick, R. J., Cohen, F. E., and Prusiner, S. B. (1993) Conversion of alpha-helices into beta-sheets features in the formation of the scrapie prion proteins. *Proc. Natl. Acad. Sci. U.S.A. 90*, 10962–10966.
3. Prusiner, S. B. (1998) Prions. *Proc. Natl. Acad. Sci. U.S.A. 95*, 13363–13383.
4. Hunter, N., Hope, J., McConnell, I., and Dickinson, A. G. (1987) Linkage of the scrapie-associated fibril protein (PrP) gene and Sinc using congenic mice and restriction fragment length polymorphism analysis. *J. Gen. Virol. 68* (Part 10), 2711–2716.
5. Peden, A. H., Head, M. W., Ritchie, D. L., Bell, J. E., and Ironside, J. W. (2004) Preclinical vCJD after blood transfusion in a PRNP codon 129 heterozygous patient. *Lancet 364*, 527–529.

6. Bishop, M. T., Hart, P., Aitchison, L., Baybutt, H. N., Plinston, C., Thomson, V., Tuzi, N. L., Head, M. W., Ironside, J. W., Will, R. G., and Manson, J. C. (2006) Predicting susceptibility and incubation time of human-to-human transmission of vCJD. *Lancet Neurol. 5*, 393–398.
7. Hunter, N. (1997) PrP genetics in sheep and the applications for scrapie and BSE. *Trends Microbiol. 5*, 331–334.
8. Bruce, M. E., McConnell, I., Fraser, H., and Dickinson, A. G. (1991) The disease characteristics of different strains of scrapie in Sinc congenic mouse lines: implications for the nature of the agent and host control of pathogenesis. *J. Gen. Virol. 72* (Part 3), 595–603.
9. Telling, G. C., Scott, M., Mastrianni, J., Gabizon, R., Torchia, M., Cohen, F. E., Dearmond, S. J., and Prusiner, S. B. (1995) Prion propagation in mice expressing human and chimeric PrP transgenes implicates the interaction of cellular PrP with another protein. *Cell 83*, 79–90.
10. Goldmann, W., Houston, F., Stewart, P., Perucchini, M., Foster, J., and Hunter, N. (2006) Ovine prion protein variant A(136)R(154)L-(168)Q(171) increases resistance to experimental challenge with bovine spongiform encephalopathy agent. *J. Gen. Virol. 87*, 3741–3745.
11. Kirby, L., Goldmann, W., Houston, F., Gill, A. C., and Manson, J. C. (2006) A novel, resistance-linked ovine PrP variant and its equivalent mouse variant modulate the in vitro cell-free conversion of rPrP to PrP(res). *J. Gen. Virol. 87*, 3747–3751.
12. Kirby, L., Birkett, C. R., Rudyk, H., Gilbert, I. H., and Hope, J. (2003) In vitro cell-free conversion of bacterial recombinant PrP to PrPres as a model for conversion. *J. Gen. Virol. 84*, 1013–1020.
13. Rezaei, H., Marc, D., Choiset, Y., Takahashi, M., Hui Bon Hoa, G., Haertle, T., Grosclaude, J., and Debey, P. (2000) High yield purification and physico-chemical properties of full-length recombinant allelic variants of sheep prion protein linked to scrapie susceptibility. *Eur. J. Biochem. 267*, 2833–2839.
14. Case, D. A., Cheatham, T. E., III, Darden, T., Gohlke, H., Luo, R., Merz, K. M., Jr., Onufriev, A., Simmerling, C., Wang, B., and Woods, R. J. (2005) The Amber biomolecular simulation programs. *J. Comput. Chem. 26*, 1668–1688.
15. Humphrey, W., Dalke, A., and Schulten, K. (1996) VMD—visual molecular dynamics. *J. Mol. Grpahics 14*, 33–38.
16. Koradi, R., Billeter, M., and Wüthrich, K. (1996) MOLMOL: a program for display and analysis of macromolecular structures, J. Mol. Graphics.
17. Riek, R., Hornemann, S., Wider, G., Billeter, M., Glockshuber, R., and Wuthrich, K. (1996) NMR structure of the mouse prion protein domain PrP(121−231). *Nature 382*, 180–182.
18. Guex, N., and Peitsch, M. C. (1997) SWISS-MODEL and the Swiss-PdbViewer: an environment for comparative protein modeling. *Electrophoresis 18*, 2714–2723.
19. Onufriev, A., Bashford, D., and Case, D. A. (2004) Exploring protein native states and large-scale conformational changes with a modified generalized born model. *Proteins 55*, 383–394.
20. Gossert, A. D., Bonjour, S., Lysek, D. A., Fiorito, F., and Wuthrich, K. (2005) Prion protein NMR structures of elk and of mouse/elk hybrids. *Proc. Natl. Acad. Sci. U.S.A. 102*, 646–650.
21. Kaneko, K., Zulianello, L., Scott, M., Cooper, C. M., Wallace, A. C., James, T. L., Cohen, F. E., and Prusiner, S. B. (1997) Evidence for protein X binding to a discontinuous epitope on the cellular prion protein during scrapie prion propagation. *Proc. Natl. Acad. Sci. U.S.A. 94*, 10069–10074.
22. Billinis, C., Panagiotidis, C. H., Psychas, V., Argyroudis, S., Nicolaou, A., Leontides, S., Papadopoulos, O., and Sklaviadis, T. (2002) Prion protein gene polymorphisms in natural goat scrapie. *J. Gen. Virol. 83*, 713–721.
23. Peletto, S., Perucchini, M., Acin, C., Dalgleish, M. P., Reid, H. W., Rasero, R., Sacchi, P., Stewart, P., Caramelli, M., Ferroglio, E., Bozzetta, E., Meloni, D., Orusa, R., Robetto, S., Gennero, S., Goldmann, W., and Acutis, P. L. (2009) Genetic variability of the prion protein gene (PRNP) in wild ruminants from Italy and Scotland. *J. Vet. Sci. 10*, 115–120.
24. Blanch, E. W., Gill, A. C., Rhie, A. G., Hope, J., Hecht, L., Nielsen, K., and Barron, L. D. (2004) Raman optical activity demonstrates poly(L-proline) II helix in the N-terminal region of the ovine prion protein: implications for function and misfunction. *J. Mol. Biol. 343*, 467–476.
25. Rhie, A., Kirby, L., Sayer, N., Wellesley, R., Disterer, P., Sylvester, I., Gill, A. C., Hope, J., James, W., and Tahiri-Alaoui, A. (2003) Characterization of 2′-fluoro-RNA aptamers that bind preferentially to disease-associated conformations of prion protein and inhibit conversion. *J. Biol. Chem. 278*, 39697–39705.
26. Rezaei, H., Eghiaian, F., Perez, J., Doublet, B., Choiset, Y., Haertle, T., and Grosclaude, J. (2005) Sequential generation of two structurally distinct ovine prion protein soluble oligomers displaying different biochemical reactivities. *J. Mol. Biol. 347*, 665–679.
27. Agrimi, U., Nonno, R., Dell'Omo, G., Di Bari, M. A., Conte, M., Chiappini, B., Esposito, E., Di Guardo, G., Windl, O., Vaccari, G., and Lipp, H. P. (2008) Prion protein amino acid determinants of differential susceptibility and molecular feature of prion strains in mice and voles. *PLoS Pathog. 4*, e1000113.
28. Gorfe, A. A., and Caflisch, A. (2007) Ser170 controls the conformational multiplicity of the loop 166−175 in prion proteins: implication for conversion and species barrier. *FASEB J. 21*, 3279–3287.
29. Sigurdson, C. J., Nilsson, K. P., Hornemann, S., Heikenwalder, M., Manco, G., Schwarz, P., Ott, D., Rulicke, T., Liberski, P. P., Julius, C., Falsig, J., Stitz, L., Wuthrich, K., and Aguzzi, A. (2009) De novo generation of a transmissible spongiform encephalopathy by mouse transgenesis. *Proc. Natl. Acad. Sci. U.S.A. 106*, 304–309.
30. Eloit, M., Adjou, K., Coulpier, M., Fontaine, J. J., Hamel, R., Lilin, T., Messiaen, S., Andreoletti, O., Baron, T., Bencsik, A., Biacabe, A. G., Beringue, V., Laude, H., Le Dur, A., Vilotte, J. L., Comoy, E., Deslys, J. P., Grassi, J., Simon, S., Lantier, F., and Sarradin, P. (2005) BSE agent signatures in a goat. *Vet. Rec. 156*, 523–524.
31. Saa, P., Castilla, J., and Soto, C. (2006) Ultra-efficient replication of infectious prions by automated protein misfolding cyclic amplification. *J. Biol. Chem. 281*, 35245–35252.
32. Bujdoso, R., Burke, D. F., and Thackray, A. M. (2005) Structural differences between allelic variants of the ovine prion protein revealed by molecular dynamics simulations. *Proteins 61*, 840–849.
33. Fitzmaurice, T. J., Burke, D. F., Hopkins, L., Yang, S., Yu, S., Sy, M. S., Thackray, A. M., and Bujdoso, R. (2008) The stability and aggregation of ovine prion protein associated with classical and atypical scrapie correlates with the ease of unwinding of helix-2. *Biochem. J. 409*, 367–375.
34. Paludi, D., Thellung, S., Chiovitti, K., Corsaro, A., Villa, V., Russo, C., Ianieri, A., Bertsch, U., Kretzschmar, H. A., Aceto, A., and Florio, T. (2007) Different structural stability and toxicity of PrP-(ARR) and PrP(ARQ) sheep prion protein variants. *J. Neurochem. 103*, 2291–2300.
35. Rezaei, H., Choiset, Y., Eghiaian, F., Treguer, E., Mentre, P., Debey, P., Grosclaude, J., and Haertle, T. (2002) Amyloidogenic unfolding intermediates differentiate sheep prion protein variants. *J. Mol. Biol. 322*, 799–814.
36. Robinson, P. J., and Pinheiro, T. J. (2009) The unfolding of the prion protein sheds light on the mechanisms of prion susceptibility and species barrier. *Biochemistry 48*, 8551–8558.
37. McCutcheon, S., Hunter, N., and Houston, F. (2005) Use of a new immunoassay to measure PrP Sc levels in scrapie-infected sheep brains reveals PrP genotype-specific differences. *J. Immunol. Methods 298*, 119–128.
38. Gayrard, V., Picard-Hagen, N., Viguie, C., Jeunesse, E., Tabouret, G., Rezaei, H., and Toutain, P. L. (2008) Blood clearance of the prion protein introduced by intravenous route in sheep is influenced by host genetic and physiopathologic factors. *Transfusion 48*, 609–619.
39. Baskakov, I., Disterer, P., Breydo, L., Shaw, M., Gill, A., James, W., and Tahiri-Alaoui, A. (2005) The presence of valine at residue 129 in human prion protein accelerates amyloid formation. *FEBS Lett. 579*, 2589–2596.
40. Bocharova, O. V., Breydo, L., Salnikov, V. V., Gill, A. C., and Baskakov, I. V. (2005) Synthetic prions generated in vitro are similar to a newly identified subpopulation of PrPSc from sporadic Creutzfeldt-Jakob disease. *Protein Sci. 14*, 1222–1232.
41. Tahiri-Alaoui, A., Gill, A. C., Disterer, P., and James, W. (2004) Methionine 129 variant of human prion protein oligomerizes more rapidly than the valine 129 variant: implications for disease susceptibility to Creutzfeldt-Jakob disease. *J. Biol. Chem. 279*, 31390–31397.
42. Simoneau, S., Rezaei, H., Sales, N., Kaiser-Schulz, G., Lefebvre-Roque, M., Vidal, C., Fournier, J. G., Comte, J., Wopfner, F., Grosclaude, J., Schatzl, H., and Lasmezas, C. I. (2007) In vitro and in vivo neurotoxicity of prion protein oligomers. *PLoS Pathog. 3*, e125.
43. Herrmann, L. M., and Caughey, B. (1998) The importance of the disulfide bond in prion protein conversion. *Neuroreport 9*, 2457–2461.